

Decentralized Stochastic Optimal Power Flow in Radial Networks with Distributed Generation

Mohammadhafez Bazrafshan, *Student Member, IEEE*, and Nikolaos Gatsis, *Member, IEEE*

Abstract—This paper develops a power management scheme that jointly optimizes the real power consumption of programmable loads and reactive power outputs of photovoltaic (PV) inverters in distribution networks. The premise is to determine the optimal demand response schedule that accounts for the stochastic availability of solar power, as well as to control the reactive power generation or consumption of PV inverters *adaptively* to the real power injections of all PV units. These uncertain real power injections by PV units are modeled as random variables taking values from a finite number of possible scenarios. Through the use of second order cone relaxation of the power flow equations, a convex stochastic program is formulated. The objectives are to minimize the negative user utility, cost of power provision, and thermal losses, while constraining voltages to remain within specified levels. To find the global optimum point, a decentralized algorithm is developed via the alternating direction method of multipliers that results in closed-form updates per node and per scenario, rendering it suitable to implement in distribution networks with large number of scenarios. Numerical tests and comparisons with an alternative deterministic approach are provided for typical residential distribution networks that confirm the efficiency of the algorithm.

Index Terms—Optimal power flow, distribution networks, photovoltaic inverters, stochastic optimization, alternating direction method of multipliers, distributed algorithms

I. INTRODUCTION

RESIDENTIAL-scale solar photovoltaic (PV) systems are paving their way into today's distribution systems, affecting higher incorporation of distributed generation into modern power systems. The chief advantage is that energy is generated closer to the point of consumption, thereby helping to reduce the transmission network congestion. A major challenge in incorporating PV systems in distribution networks is the uncertain availability of solar energy due to changes in irradiance conditions. These changes lead to insufficient or at times excess electricity generation, and if unaccounted for, can result in reduced user satisfaction, poor voltage regulation, and eventually equipment failure.

To deal with these issues, programmable loads that enable control of their real power consumption provide an opportunity for distribution system operators (DSO) to reduce the peak load in periods of inadequate generation. Moreover, reactive power generation or consumption by PV inverters, which provide the AC interface between the PV system and the grid, can be leveraged to improve voltage regulation. Although

current standards prohibit these inverters to operate at a variable power factor [1], the potential advantages of using these capabilities for voltage regulation have been extensively reported in literature; see e.g., [2]–[4].

Building upon the aforementioned capabilities, this paper proposes a decentralized real and reactive power management framework in distribution systems with high levels of PV generation. To account for the inherent uncertainty in solar power generation, stochastic programming tools [5] are used to achieve common objectives such as loss minimization, operational cost reduction, and acceptable voltage regulation.

A. Prior Art

Power management in distribution networks amounts to an optimal power flow (OPF) problem that minimizes certain objectives subject to power flow equations that are generally nonconvex. See [6]–[8], for the canonical form of power flow equations in radial distribution networks. Due to the nonconvexity of power flow equations, many relaxations and approximations have been recently proposed. A comprehensive study summarizing the recent advances in convex relaxations of OPF can be found in [9] and [10]. In particular, conic relaxation techniques are used in [11] for radial distribution load flow, while [12], [13], and [14] provide conditions to guarantee optimality of relaxations to the original OPF.

Deterministic approaches to reactive power management in distribution networks have recently been investigated in many studies where user power consumption and PV power generation are known. The reactive power management problem is approached in [15], [16], and [2] using a linear approximation of the power flow equations, called `LinDistFlow` equations, and local reactive power control policies. Although these local policies are computationally attractive and perform well in practical scenarios, they do not provide optimality guarantees.

An optimal decentralized algorithm for solving the reactive power control problem under the `LinDistFlow` model is developed in [17] using the alternating direction method of multipliers (ADMM). An adaptive VAR control scheme is pursued in [18] based on the `LinDistFlow` where the adaptation law switches between minimizing power losses or maintaining voltage regulation. Centralized reactive power control and PV inverter loss minimization using the second-order cone programming (SOCP) relaxation is the theme of [19].

Decentralized solvers for real and reactive power optimization using the SOCP relaxations are developed in [20] and [21] using the Predictor Corrector Proximal Method of Multipliers (PCPM). Leveraging the SOCP relaxation and the ADMM,

Manuscript received February 9, 2015; revised June 12, 2015 and October 30, 2015; accepted January 4, 2016.

The authors are with the department of electrical and computer engineering, the University of Texas at San Antonio, San Antonio, TX 78249, USA (emails: aju084@my.utsa.edu, nikolaos.gatsis@utsa.edu)

This material is based upon work supported by the National Science Foundation under Grant No. CCF-1421583.

a decentralized solver for OPF with closed-form updates is designed in [22] where the user-consumed reactive power is modeled as independent of users' real power consumption. Decentralized real power control using ADMM with convex envelop approximations is developed in [23]. Leveraging semidefinite programming (SDP) relaxations, decentralized algorithms are designed in [24] and [25] using ADMM, and in [26] via a dual subgradient method. Distributed reactive power control is performed in [27] with the purpose of maintaining nodal voltages within specification limits.

A nonconvex formulation for the reactive power control problem is presented in [28], and a solver based on sequential convex programming is developed, but without global optimality guarantees. An adaptive local learning algorithm is devised in [4] which provides a fast approximate solution for voltage regulation using the solutions of past optimizations.

Up to this point, all previously mentioned approaches assume that real power injections in buses with renewable generation are known, and hence are deterministic. The works in [29] and [30] propose distributed online algorithms for optimal reactive power compensation and loss minimization based on feedback control from local voltage measurements. By modeling local voltages as functions of reactive power in microgenerators, the loss terms are casted as a quadratic form in reactive powers, and a modified dual method is used to minimize the losses subject to power constraints. These works model the real power injection of distributed generators as unmeasured disturbances.

In this light, the work in [31] also assumes no knowledge of the real power injection of distributed generators. It is shown that a purely local reactive power control that leverages only voltage measurements and does not rely on communication, does not by itself guarantee acceptable voltage regulation. Therefore, to perform voltage regulation and provide optimality guarantees, additional information, such as previous control inputs is incorporated in their proposed algorithm.

The work in [32] models loads and real power injections on nodes as stochastic processes, collects noisy and delayed estimates of those, and decides the reactive power injection by solving a centralized optimization problem using a stochastic approximation algorithm. Uncertainty-aware optimal real and reactive power management from PV units is analyzed in [33] where the conditional-value-at-risk is utilized to minimize the risk of overvoltages.

B. Contributions and outline

The contributions of this paper are as follows:

- 1) An optimal power flow problem for distribution networks accounting for the uncertainty in solar generation is formulated. In particular, the real powers generated by PV units at different nodes are modeled as random variables that take values from a finite set of scenarios. Real power of user controllable loads is optimized jointly with reactive power injection or absorption by PV inverters and network power flows per scenario. This stochastic model captures the uncertainty in solar generation which is not accounted for in previous approaches [2]–[4] and [15]–[28], which assume known (deterministic) PV injections.

In contrast to [29]–[31], in which voltage regulation through reactive power control is based on feedback from local voltage measurements, our methodology maintains voltages within specified limits while accounting for the underlying uncertainty of the PV generation. Recently, uncertainty in distributed PV generation has been addressed in [33] and [32]. Reactive power control by PV units and power flows are decided in the present work adaptively to solar power outputs, as opposed to a static fashion in [33]. User controllable loads are not modeled in [32], which in addition features a centralized optimization scheme, in contrast to the decentralized solution algorithm developed here (featured as the second contribution next).

- 2) This paper develops a decentralized solver with the following desirable attributes, motivated by scalability considerations: (a1) updates are decomposed per node and per scenario; (a2) all updates are in closed-form and (a3) communication only between neighboring nodes is required. The decentralized algorithm is based on ADMM. Even though ADMM naturally lends itself to distributed computation, there are two challenges that need to be addressed, in order to successfully arrive to an optimization algorithm with the previously mentioned attributes: (c1) introduce properly designed auxiliary variables, and (c2) appropriately split the set of constraints into coupling and individual constraints. Different choices for (c1) and (c2) may lead to entirely different algorithms; one of this paper's contributions is to address those challenges towards a fully decentralized solver with closed-form updates. The decentralization methodology in this paper is extending the ADMM approach in [22] in a stochastic programming setup. In addition, the closed-form solution of an SOCP in 4 variables with upper bounds on certain variables is derived, motivated by the incorporation of line current limits in the present formulation. This paper also expands previous work in [34]—which featured only single-line networks and the LinDistFlow approximations—in two major ways: (1) SOCP relaxation of power flow equations is incorporated, which is a more complex but also more accurate model; and (2) the formulation incorporates tree networks.
- 3) Considering realistic PV generation models and only a small number of representative scenarios for the uncertainty, numerical tests highlight the benefits of the proposed stochastic formulation with regards to user satisfaction and thermal loss minimization. Improved voltage regulation and reduced thermal losses are demonstrated in comparison to alternative distributed control schemes in [2], and also in networks that include shunt capacitors.

The remainder of this paper is organized as follows. Section II introduces the network model, the decision variables, and pertinent constraints. The optimization problem is formulated in Section III. Section IV develops the equivalent formulation suitable for decentralized solution by the ADMM, and derives the closed-form updates. Section V deliberates on the algorithm implementation and the communication requirements.

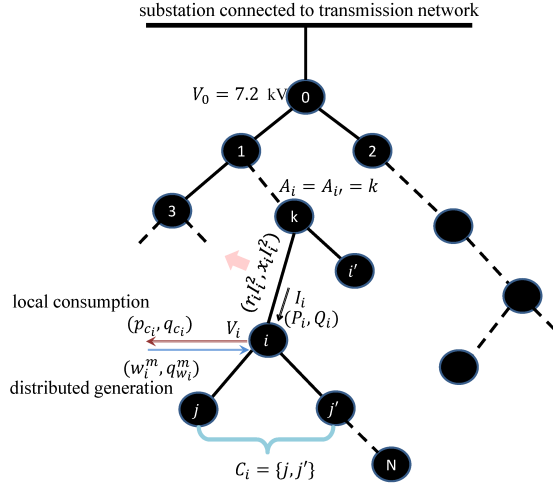


Fig. 1. A radial distribution network modeled as a tree graph.

Numerical tests are provided in Section VI as well as comparisons with competing approaches. Section VII concludes the paper.

II. NETWORK MODEL AND DECISION VARIABLES

Consider a radial distribution network as depicted in Fig. 1 modeled by a tree graph, where the set of all nodes is denoted as $\mathcal{N} = \{0, 1, 2, \dots, N\}$. Node 0 (i.e., root of the graph) is the substation connected to the transmission network, and the remaining N nodes represent users.

Following the tree model for distribution networks, each node $i \in \mathcal{N} \setminus \{0\}$ has a unique ancestor denoted by A_i . The line connecting node A_i to node i is labeled as line i , and is considered to have resistance r_i and reactance x_i . Each node $i \in \mathcal{N}$ has an associated set of child nodes denoted by \mathcal{C}_i . For the terminal nodes (i.e., leaves of the tree, or nodes without children), it holds that $\mathcal{C}_i = \emptyset$.

A. User load model

User i consumes a non-elastic real and reactive load denoted by P_{L_i} and Q_{L_i} respectively. Moreover, users are supposed to have demand response capabilities, and their elastic consumption p_{c_i} is permitted to vary in a certain range:

$$0 \leq p_{c_i} \leq p_{c_i}^{\max}, \quad i \in \mathcal{N} \setminus \{0\}. \quad (1)$$

The elastic reactive power consumption q_{c_i} has a linear relationship with the real power p_{c_i} :

$$q_{c_i} = \left(\sqrt{\frac{1}{\text{PF}_i^2} - 1} \right) p_{c_i}, \quad i \in \mathcal{N} \setminus \{0\}. \quad (2)$$

where PF_i is the power factor, a dimensionless number in the interval $(0, 1]$.

B. PV generation model

User nodes may also be enabled with PV generation. Attributable to the stochastic nature of solar power, the real power injections of PV systems are modeled as random

variables. The real power injections across the network take values from a finite set of M possible scenarios, each with probability π^m , with $m \in \mathcal{M} = \{1, 2, \dots, M\}$. It is thus assumed that the real power generated by the PV unit at node i and in scenario m is given by w_i^m . A typical probabilistic model for generating scenarios is the beta distribution, see e.g., [35] and [36]. The mean value of the distribution can be set to a forecasted generation for the next time period that could range from e.g., 15 minutes to 1 hour.

The DC electrical output generated by the PV modules are translated into an AC output through the use of PV inverters. These PV inverters are also capable of generating or consuming reactive power by themselves; see e.g., [2]. Let $q_{w_i}^m$ denote the reactive power generated by the PV inverter at node i in scenario m . Then, $q_{w_i}^m$ is a decision variable constrained by

$$-q_{w_i}^{\max} \leq q_{w_i}^m \leq q_{w_i}^{\max}, \quad i \in \mathcal{N} \setminus \{0\}, m \in \mathcal{M} \quad (3)$$

where $q_{w_i}^{\max} = \sqrt{s_{w_i}^2 - (w_i^m)^2}$ and s_{w_i} is the maximum apparent power capacity of the PV at node i , that is, the nameplate capacity of the PV inverter at that node.

C. Power flow equations

The scenario-dependency of real and reactive power injections of PV units renders the power flow equations across the network to be scenario dependent as well. At scenario m , real and reactive power flows on line i are denoted by P_i^m and Q_i^m respectively; the squared magnitude of the voltage phasor at node i and the squared magnitude of the current phasor on line i are represented by v_i^m and l_i^m , respectively. The power flow equations leveraging the SOCP relaxation are as follows, where all the constraints hold for $m \in \mathcal{M}$ and $i \in \mathcal{N}$:

$$P_i^m = \sum_{j \in \mathcal{C}_i} (P_j^m + r_j l_j^m) + P_{L_i} + p_{c_i} - w_i^m \quad (4)$$

$$Q_i^m = \sum_{j \in \mathcal{C}_i} (Q_j^m + x_j l_j^m) + Q_{L_i} + q_{c_i} - q_{w_i}^m - q_{s_i} v_i^m \quad (5)$$

$$v_{A_i}^m = v_i^m + 2(r_i P_i^m + x_i Q_i^m) + (r_i^2 + x_i^2) l_i^m, i \neq 0, \quad (6)$$

$$(P_i^m)^2 + (Q_i^m)^2 \leq v_i^m l_i^m, i \neq 0, \quad (7)$$

$$v_i^m \geq 0, i \neq 0. \quad (8)$$

In the equations above, r_i and x_i have units of Ω . Real powers have units of MW and reactive powers are in MVars. Square currents are in $(kA)^2$ while square magnitude of voltages v_i^m have units of $(kV)^2$. Note that $v_i^m = (V_i^m)^2$ where V_i^m is the magnitude of the voltage phasor at node i and scenario m . The substation voltage is fixed at $v_0 = v_0^m = (V_0^m)^2$ and since there is no user at the substation, $p_{c_0}, w_0^m, q_{w_0}^m$ are all zero.

The power flow equations (4)-(8) clearly show that fluctuations in solar real power injection (w_i^m) ultimately lead to variations in voltage levels (v_i^m) across nodes in the network. In order to guarantee that node voltages remain within safety levels, the following voltage regulation constraint is enforced at every node $i \in \mathcal{N} \setminus \{0\}$ per scenario $m \in \mathcal{M}$

$$(1 - \epsilon)^2 \leq \frac{v_i^m}{v_0} \leq (1 + \epsilon)^2 \quad (9)$$

TABLE I
DECISION VARIABLES, USER AND NETWORK PARAMETERS

Decision variables	
Scenario-independent	p_{c_i}, q_{c_i}
Scenario-dependent	$P_i^m, Q_i^m, v_i^m, l_i^m, q_{w_i}^m$
Parameters (known)	
User	$P_{L_i}, Q_{L_i}, \text{PF}_i, p_{c_i}^{\max}, w_i^m, s_{w_i}$
Network	$r_i, x_i, q_{s_i}, \epsilon, l_i^{\max}$

where ϵ could be chosen to be 0.05. The current magnitudes for every line are capped as per the following constraint:

$$0 \leq l_i^m \leq l_i^{\max}. \quad (10)$$

A summary of decision variables along with the user and network parameters is given in Table I.

Having described the optimization variables and constraints, the next section elaborates on the relevant objective function and completes the problem formulation.

III. OPTIMAL POWER FLOW FORMULATION

One of the main objectives for a DSO is to meet customer demand. In order to quantify user satisfaction for demand response decisions, a concave utility function denoted as $u_i(p_{c_i})$ is adopted for each user i . Maximizing the sum of user utilities hence constitutes the first objective.

Power flows in the network are provided through the substation that is connected to the transmission grid. The DSO undergoes a cost to obtain this power from the transmission network. Although any cost function $C(P_0^m)$ that is convex can be used to evaluate the cost of power provision at scenario m , a particular cost function of interest could be one that distinguishes between the buying price (import) and the selling price (export). One such example is a piece-wise linear function of the form:

$$C(P_0^m) = \begin{cases} aP_0^m & \text{if } P_0^m \geq 0 \\ bP_0^m & \text{if } P_0^m < 0 \end{cases} \quad (11)$$

with $a > b \geq 0$ to preserve convexity. The expected value of $C(P_0^m)$ over all scenarios, that is $\sum_{m=1}^M \pi^m C(P_0^m)$ is the second term in the objective. The third term in the objective is the expected incurred thermal losses in the lines over all the scenarios, that is $\sum_{m=1}^M \pi^m \sum_{i=1}^N r_i l_i^m$.

Let $\mathbf{P}, \mathbf{Q}, \mathbf{v}, \mathbf{l}, \mathbf{p}_c, \mathbf{q}_w$ collect the respective variables per node and per scenario (if the variable is scenario dependent). The optimization problem amounts to

$$\begin{aligned} \min_{\substack{\mathbf{P}, \mathbf{Q}, \mathbf{v} \\ \mathbf{l}, \mathbf{p}_c, \mathbf{q}_w}} & - \sum_{i=1}^N u_i(p_{c_i}) + \sum_{m=1}^M \pi^m C(P_0^m) \\ & + K_{\text{Loss}} \sum_{m=1}^M \pi^m \sum_{i=1}^N r_i l_i^m \end{aligned} \quad (12)$$

subject to (1) – (10)

where $K_{\text{Loss}} \geq 0$ is a weight which can be selected by the system operator to reflect the relative priority of loss minimization with respect to the two other objective terms.

Problem (12) forms a two-stage stochastic convex program with first-and-second-stage decisions. First-stage decisions are determined independently of the uncertainty and comprise elastic load consumptions p_{c_i} 's (and ultimately q_{c_i} 's). Second-stage decisions are determined adaptively to the uncertainty and include reactive power injection/absorption provided by the PV inverters ($q_{w_i}^m$), power flows (P_i^m, Q_i^m), and squared magnitude of voltages and currents (v_i^m and l_i^m for every scenario).

Remark (Compatibility of the formulation with any convex cost function). Auxiliary variables can be used to relieve the difficulty of directly working with piecewise linear (nondifferentiable) functions such as (11) in the objective. For example, $C(P_0^m)$ can be written as

$$C(P_0^m) = aP_{0+}^m - bP_{0-}^m \quad (13)$$

and the following constraints are added (for $m \in \mathcal{M}$):

$$P_0^m = P_{0+}^m - P_{0-}^m, \quad P_{0+}^m \geq 0, P_{0-}^m \geq 0. \quad (14)$$

Solving (12) with $C(P_0^m)$ given by (13) and with added constraints of (14) is equivalent to solving (12) with $C(P_0^m)$ given by (11). The advantage of the former approach is that it includes a smooth objective. Appendix A proves the equivalence by showing that solving (12) with $C(P_0^m)$ given by (13) ensures that only one of the variables (P_{0+}^m, P_{0-}^m) is nonzero per scenario m . This implies that either $P_0^m = P_{0+}^m > 0$, or $P_0^m = -P_{0-}^m < 0$. For the algorithm that is to be presented, this particular cost function is considered as an example since it is more challenging to deal with. For a differentiable convex function, only one variable (P_0^m) is needed to be considered, which yields simpler updates.

Remark (Optimality of second-order cone stochastic program). The second-order cone relaxation of OPF has been proved to be exact for tree networks under certain assumptions [14]. By applying the techniques developed in [14], sufficient conditions under which the inequality in (7) holds as equality for the convex stochastic program (12) are derived in Appendix B.

The two-stage convex stochastic program (12) developed in this section can be solved by centralized algorithms such as interior point methods. In the next section, a decentralized solver for (12) based on ADMM is developed featuring closed-form updates per node and per scenario.

IV. SOLUTION ALGORITHM

The detailed design of the decentralized solution algorithm is presented in this section. An equivalent problem to (12) which is of the general form amenable to application of ADMM is derived in Subsection IV-A. This equivalent problem includes judiciously designed auxiliary variables that allow decomposition per node and per scenario. Subsection IV-B, briefly outlines the ADMM. Finally, in Subsection IV-C, the closed-form updates per node and per scenario are detailed.

A. Equivalent problem

The only obstacle in fully decomposing (12) into separate nodes is the coupling in power flow equations (4)-(6). For instance, in (4) and (5), node i will need to know P_j^m , Q_j^m , and l_j^m from child nodes $j \in \mathcal{C}_i$. In order to decouple each node from its child nodes, N respective copies of these variables, \hat{P}_j^m , \hat{Q}_j^m , and \hat{l}_j^m are introduced per scenario. Moreover, since all nodes except for the root have ancestors, constraint (6) is also coupling the nodes. Therefore, per scenario, another set of N variables \hat{v}_i^m copies $v_{A_i}^m$ at node i . Finally, an additional set of copies per scenario, namely, \tilde{P}_i^m , \tilde{Q}_i^m , \tilde{l}_i^m , and \tilde{v}_i^m for all $n \in \mathcal{N} \setminus \{0\}$ and the variables \tilde{P}_{0+}^m , \tilde{P}_{0-}^m for the root, are also introduced, the purpose of which will be evident shortly.

Let the set of boldface variables $\{\mathbf{P}, \hat{\mathbf{P}}, \tilde{\mathbf{P}}, \mathbf{Q}, \hat{\mathbf{Q}}, \tilde{\mathbf{Q}}, \mathbf{v}, \hat{\mathbf{v}}, \tilde{\mathbf{v}}, \mathbf{l}, \hat{\mathbf{l}}, \tilde{\mathbf{l}}, \mathbf{p}_c, \hat{\mathbf{p}}_c, \mathbf{q}_w, \hat{\mathbf{q}}_w, \mathbf{P}_{0+}, \mathbf{P}_{0-}, \tilde{\mathbf{P}}_{0+}, \tilde{\mathbf{P}}_{0-}\}$ represent vectors collecting the corresponding variables in all scenarios and nodes. As listed in Table II, these variables are further collected in vectors $\mathbf{x} = \{\mathbf{x}_i^m\}_{i \in \mathcal{N}, m \in \mathcal{M}}$ and $\mathbf{z} = \{\mathbf{z}_i^m\}_{i \in \mathcal{N}, m \in \mathcal{M}}$.

The problem takes the following form:

$$\min_{\mathbf{x}, \mathbf{z}} - \sum_{i=1}^N u_i(\tilde{p}_{c_i}) + \sum_{m=1}^M \pi^m (aP_{0+}^m - bP_{0-}^m) + K_{\text{Loss}} \sum_{m=1}^M \pi^m \sum_{i=1}^N r_i l_i^m \quad (15a)$$

subject to:

Coupling Constraints ($i \in \mathcal{N}, m \in \mathcal{M}$):

$$i \neq 0: \quad P_i^m = \tilde{P}_i^m \quad Q_i^m = \tilde{Q}_i^m \quad l_i^m = \tilde{l}_i^m \quad (15b)$$

$$v_i^m = \tilde{v}_i^m \quad \hat{v}_i^m = \tilde{v}_{A_i}^m \quad p_{c_i}^m = \tilde{p}_{c_i}^m \quad q_{w_i}^m = \tilde{q}_{w_i}^m \quad (15c)$$

$$j \in \mathcal{C}_i: \quad \hat{P}_j^m = \tilde{P}_j^m \quad \hat{Q}_j^m = \tilde{Q}_j^m \quad \hat{l}_j^m = \tilde{l}_j^m \quad (15d)$$

$$P_{0+}^m = \tilde{P}_{0+}^m \quad P_{0-}^m = \tilde{P}_{0-}^m \quad (15e)$$

Individual Equality Constraints ($i \in \mathcal{N}, m \in \mathcal{M}$):

$$P_i^m = \sum_{j \in \mathcal{C}_i} (\hat{P}_j^m + r_j \hat{l}_j^m) + P_{L_i} + p_{c_i}^m - w_i^m \quad (15f)$$

$$Q_i^m = \sum_{j \in \mathcal{C}_i} (\hat{Q}_j^m + x_j \hat{l}_j^m) + Q_{L_i} + q_{c_i}^m - q_{w_i}^m - q_{s_i} v_i^m \quad (15g)$$

$$\hat{v}_i^m = v_i^m + 2(r_i P_i^m + x_i Q_i^m) + (r_i^2 + x_i^2) l_i^m, i \neq 0 \quad (15h)$$

where $q_{c_i}^m = \left(\sqrt{\frac{1}{\text{PF}_i^2}} - 1 \right) p_{c_i}^m$.

$$P_{0+}^m = P_{0+}^m - P_{0-}^m \quad (15i)$$

Individual Inequality Constraints ($i \in \mathcal{N}, m \in \mathcal{M}$):

$$(\tilde{P}_i^m)^2 + (\tilde{Q}_i^m)^2 \leq (\tilde{v}_i^m)(\tilde{l}_i^m), i \neq 0 \quad (15j)$$

$$(1 - \epsilon)^2 \leq \frac{\tilde{v}_i^m}{v_0} \leq (1 + \epsilon)^2, i \neq 0 \quad (15k)$$

$$0 \leq \tilde{l}_i^m \leq l_i^{\max}, i \neq 0 \quad (15l)$$

$$p_{c_i}^{\min} \leq \tilde{p}_{c_i} \leq p_{c_i}^{\max} \quad (15m)$$

$$-q_{w_i}^{\max} \leq \tilde{q}_{w_i}^m \leq q_{w_i}^{\max} \quad (15n)$$

$$\tilde{P}_{0+}^m \geq 0, \tilde{P}_{0-}^m \geq 0. \quad (15o)$$

Clearly, (15) is equivalent to (12).

TABLE II
X AND Z VARIABLES FOR THE ADMM ALGORITHM

	Nodes involved	Variables
\mathbf{x}_0^m	Root	$\{P_0^m, Q_0^m, P_{0+}^m, P_{0-}^m, \hat{P}_j^m, \hat{Q}_j^m, \hat{l}_j^m\}_{j \in \mathcal{C}_0}\}$
\mathbf{x}_i^m	Neither root nor leaf	$\{P_i^m, Q_i^m, v_i^m, l_i^m, \hat{P}_j^m, \hat{Q}_j^m, \hat{l}_j^m\}_{j \in \mathcal{C}_i}, \hat{v}_i^m, p_{c_i}^m, q_{w_i}^m\}$
\mathbf{x}_i^m	Leaf	$\{P_i^m, Q_i^m, v_i^m, l_i^m, \hat{v}_i^m, p_{c_i}^m, q_{w_i}^m\}$
\mathbf{x}_i	All nodes	$\{\mathbf{x}_i^m\}_{m=1}^M$
\mathbf{z}_0^m	Root	$\{\tilde{P}_{0+}^m, \tilde{P}_{0-}^m\}$
\mathbf{z}_i^m	Not root	$\{\tilde{P}_i^m, \tilde{Q}_i^m, \tilde{v}_i^m, \tilde{l}_i^m, \tilde{q}_{w_i}^m\}$
\mathbf{z}_i	Not root	$\{\{\mathbf{z}_i^m\}_{m=1}^M, \tilde{p}_{c_i}\}$

B. Review of ADMM

With the previous definitions of \mathbf{x} and \mathbf{z} , problem (15) is of the general form [37]

$$\min_{\mathbf{x} \in \mathcal{X}, \mathbf{z} \in \mathcal{Z}} f(\mathbf{x}) + g(\mathbf{z}) \quad \text{subj. to} \quad A\mathbf{x} + B\mathbf{z} = \mathbf{c} \quad (16)$$

where f and g are convex functions. The set \mathcal{X} corresponds to the individual equality constraints (15f)-(15i) and \mathcal{Z} captures all the inequality constraints (15j)-(15o).

The augmented Lagrangian function is defined as:

$$L_\rho(\mathbf{x}, \mathbf{z}, \mathbf{y}) = f(\mathbf{x}) + g(\mathbf{z}) + \mathbf{y}^T (A\mathbf{x} + B\mathbf{z} - \mathbf{c}) + \frac{\rho}{2} \|A\mathbf{x} + B\mathbf{z} - \mathbf{c}\|_2^2 \quad (17)$$

where \mathbf{y} is the Lagrange multiplier vector for the linear equality constraints in (16), and $\rho > 0$ is a parameter. The primal and dual iterations of ADMM are as follows, where k is the iteration index.

$$\mathbf{x}(k+1) := \underset{\mathbf{x} \in \mathcal{X}}{\text{argmin}} L_\rho(\mathbf{x}, \mathbf{z}(k), \mathbf{y}(k)) \quad (18)$$

$$\mathbf{z}(k+1) := \underset{\mathbf{z} \in \mathcal{Z}}{\text{argmin}} L_\rho(\mathbf{x}(k+1), \mathbf{z}, \mathbf{y}(k)) \quad (19)$$

$$\mathbf{y}(k+1) := \mathbf{y}(k) + \rho [A\mathbf{x}(k+1) + B\mathbf{z}(k+1) - \mathbf{c}]. \quad (20)$$

The purpose of introducing the *tilde* variables in (15) is so that the individual inequality constraints in \mathcal{Z} can be handled separately in the \mathbf{z} -update. The \mathbf{x} -update on the other hand turns out to be an equality constrained quadratic program. This separation of variables are essential to finding closed-form solutions for the updates. The following primal and dual residuals are measured in every step, and the algorithm is stopped once these are below an acceptable threshold:

$$r(k) := \|A\mathbf{x}(k) + B\mathbf{z}(k) - \mathbf{c}\| \quad (21a)$$

$$s(k) := \rho \|A^T B(\mathbf{z}(k) - \mathbf{z}(k-1))\|. \quad (21b)$$

C. Updates

The Lagrange multipliers corresponding to the coupling constrains of (15b)-(15e) are listed in Table III. To perform ADMM, first the Augmented Lagrangian (17) for problem (15) needs to be formed. This Augmented Lagrangian is separable across variables \mathbf{x}_i^m ($i \in \mathcal{N}, m \in \mathcal{M}$) with \mathbf{z} fixed, or across variables \mathbf{z}_i^m and \tilde{p}_{c_i} ($i \in \mathcal{N}, m \in \mathcal{M}$) with \mathbf{x} fixed. Each

step of the ADMM will consist of minimizing the augmented Lagrangian with respect to either \mathbf{x} or \mathbf{z} and updating the Lagrange multipliers.

1) \mathbf{x}_i^m -update: For node $i \in \mathcal{N} \setminus \{0\}$, per scenario m , the \mathbf{x} -update will be derived by minimizing the corresponding part of the augmented Lagrangian per node i and scenario m :

$$\begin{aligned} \min_{\mathbf{x}_i^m} & K_{\text{Loss}} \pi^m r_i l_i^m + \lambda_i^m (P_i^m - \tilde{P}_i^m) + \sum_{j \in \mathcal{C}_i} \hat{\lambda}_j^m (\hat{P}_j^m - \tilde{P}_j^m) \\ & + \mu_i^m (Q_i^m - \tilde{Q}_i^m) + \sum_{j \in \mathcal{C}_i} \hat{\mu}_j^m (\hat{Q}_j^m - \tilde{Q}_j^m) + \gamma_i^m (l_i^m - \tilde{l}_i^m) \\ & + \sum_{j \in \mathcal{C}_i} \hat{\gamma}_j^m (\hat{l}_j^m - \tilde{l}_j^m) + \omega_i^m (v_i^m - \tilde{v}_i^m) + \sum_{j \in \mathcal{C}_i} \hat{\omega}_j^m (\hat{v}_j^m - \tilde{v}_j^m) \\ & + \eta_i^m (p_{c_i}^m - \tilde{p}_{c_i}) + \theta_i^m (q_{w_i}^m - \tilde{q}_{w_i}) + \frac{\rho}{2} [(P_i^m - \tilde{P}_i^m)^2 \\ & + \sum_{j \in \mathcal{C}_i} (\hat{P}_j^m - \tilde{P}_j^m)^2 + (Q_i^m - \tilde{Q}_i^m)^2 + \sum_{j \in \mathcal{C}_i} (\hat{Q}_j^m - \tilde{Q}_j^m)^2 \\ & + (l_i^m - \tilde{l}_i^m)^2 + \sum_{j \in \mathcal{C}_i} (\hat{l}_j^m - \tilde{l}_j^m)^2 + (v_i^m - \tilde{v}_i^m)^2 \\ & + \sum_{j \in \mathcal{C}_i} (\hat{v}_j^m - \tilde{v}_j^m)^2 + (p_{c_i}^m - \tilde{p}_{c_i})^2 + (q_{w_i}^m - \tilde{q}_{w_i})^2] \end{aligned} \quad (22)$$

subject to (15f) – (15h).

For the special case of $i = 0$, the corresponding Lagrangian will include the term $\pi^m (aP_{0+}^m - bP_{0-}^m) + \frac{\rho}{2} [(P_{0+}^m - \tilde{P}_{0+}^m)^2 + (P_{0-}^m - \tilde{P}_{0-}^m)^2]$ with the constraint $P_{0+}^m = P_{0+}^m - P_{0-}^m$.

For all $i \in \mathcal{N}$ problem (22) is of the following form:

$$\frac{1}{2} (\mathbf{x}_i^m)^T \mathbf{A}_i^m \mathbf{x}_i^m + (\mathbf{b}_i^m)^T \mathbf{x}_i^m \quad \text{subj. to } \mathbf{C}_i^m \mathbf{x}_i^m = \mathbf{d}_i^m. \quad (23)$$

The structure of the problem leads to a diagonal \mathbf{A}_i^m and a full-rank \mathbf{C}_i^m , and therefore has a closed-form solution:

$$\mathbf{x}_i^{m*} = \mathbf{A}_i^{m-1} (-\mathbf{b}_i^m + \mathbf{C}_i^{mT} \mathbf{F}_i^m) \quad (24)$$

where $\mathbf{F}_i^m = (\mathbf{C}_i^m \mathbf{A}_i^{m-1} \mathbf{C}_i^{mT})^{-1} (\mathbf{d}_i^m + \mathbf{C}_i^m \mathbf{A}_i^{m-1} \mathbf{b}_i^m)$.

2) \mathbf{z}_i -update: In order to find the updates for \mathbf{z}_i^m -variables the augmented Lagrangian in (17) can be minimized separately for $\{\tilde{P}_i^m, \tilde{Q}_i^m, \tilde{v}_i^m, \tilde{l}_i^m\}$, \tilde{p}_{c_i} , \tilde{q}_{w_i} , \tilde{P}_{0+} , and \tilde{P}_{0-} per $i \in \mathcal{N}$ and $m \in \mathcal{M}$ subject to (15j)-(15o).

The minimization with respect to $\{\tilde{P}_i^m, \tilde{Q}_i^m, \tilde{v}_i^m, \tilde{l}_i^m\}$ has a closed-form solution which is developed in Appendix C by generalizing [22, Appendix I].

The variable \tilde{p}_{c_i} is not dependent on the scenario, and its update is by solving the following program at every node:

$$\begin{aligned} \tilde{p}_{c_i} = \underset{0 \leq \tilde{p}_{c_i} \leq p_{c_i}^{\max}}{\text{argmin}} & \left[u_i(\tilde{p}_{c_i}) + \sum_{m=1}^M \eta_i^m (p_{c_i}^m - \tilde{p}_{c_i}) \right. \\ & \left. + \frac{\rho}{2} \sum_{m=1}^M (p_{c_i}^m - \tilde{p}_{c_i})^2 \right]. \end{aligned} \quad (25)$$

This problem is a scalar box-constrained convex optimization problem, and has a closed-form solution if e.g., the utility function is quadratic. The remaining \mathbf{z} -variables, namely $\tilde{q}_{w_i}^m$, \tilde{P}_{0+}^m , and \tilde{P}_{0-}^m , are scenario dependent, and their closed-form updates are given as follows (by minimizing the corresponding

TABLE III
LAGRANGE MULTIPLIERS

Equality Constraint	Lagrange Multiplier
$P_i^m = \tilde{P}_i^m$	λ_i^m
$Q_i^m = \tilde{Q}_i^m$	μ_i^m
$l_i^m = \tilde{l}_i^m$	γ_i^m
$v_i^m = \tilde{v}_i^m$	ω_i^m
$\hat{v}_j^m = \tilde{v}_{A_j}^m$	$\hat{\omega}_j^m$
$\hat{P}_j^m = \tilde{P}_{j \in \mathcal{C}_i}^m$	$\hat{\lambda}_j^m$
$\hat{Q}_j^m = \tilde{Q}_{j \in \mathcal{C}_i}^m$	$\hat{\mu}_j^m$
$\hat{l}_j^m = \tilde{l}_{j \in \mathcal{C}_i}^m$	$\hat{\gamma}_j^m$
$p_{c_i}^m = \tilde{p}_{c_i}$	η_i^m
$q_{w_i}^m = \tilde{q}_{w_i}$	θ_i^m
$P_{0+}^m = \tilde{P}_{0+}^m$	ζ_+^m
$P_{0-}^m = \tilde{P}_{0-}^m$	ζ_-^m

term in the Lagrangian):

$$\tilde{q}_{w_i}^m(k+1) = \left[\frac{\theta_i^m + \rho q_{w_i}^m}{\rho} \right]_{-q_{w_i}^{\max}}^{q_{w_i}^{\max}} \quad (26)$$

$$\tilde{P}_{0+}^m(k+1) = \left[\frac{\zeta_+^m + \rho P_{0+}^m}{\rho} \right]^+ \quad (27)$$

$$\tilde{P}_{0-}^m(k+1) = \left[\frac{\zeta_-^m + \rho P_{0-}^m}{\rho} \right]^+ \quad (28)$$

where $[t]^+ := \max\{0, t\}$ and $[t]_{t_1}^{t_2} := \max\{t_1, \min\{t, t_2\}\}$.

Following the detailed derivation of the ADMM-based algorithm in the present section, the next section deals with the implementation of the algorithm in a distributed fashion, and highlights its advantages.

V. DECENTRALIZED IMPLEMENTATION

In the implementation of this algorithm, each node $i \in \mathcal{N}$ is responsible for maintaining and updating variables \mathbf{x}_i , \mathbf{z}_i , and the corresponding Lagrange multipliers.

The ADMM algorithm works as depicted in Fig. 2. First, \mathbf{z} and the Lagrange multipliers are initialized with arbitrary numbers. In each iteration, every node i that has children receives \tilde{P}_j^m , \tilde{Q}_j^m , and \tilde{l}_j^m from all $j \in \mathcal{C}_i$. Also, each node i receives $\tilde{v}_{A_i}^m$ from its ancestor. Using these variables, \mathbf{x}_i^m is updated according to the closed-form solution in (24).

Prior to the \mathbf{z} -update step, \tilde{P}_i^m , \tilde{Q}_i^m , and \tilde{l}_i^m are sent to node i from ancestor A_i , and node i collects $\{\hat{v}_j^m\}_{j \in \mathcal{C}_i}$ from its children. Upon receiving the required information, node i performs the \mathbf{z} -update step. Upon completion of the \mathbf{z} -update step, the Lagrange multipliers are updated.

Note that, node 0 only communicates with its children, and the leaf nodes only communicate with their ancestors. All other nodes communicate both with their children and ancestors. Therefore in this algorithm only neighbors will need to communicate.

Algorithm 1 summarizes the algorithm. Convergence in Step 2 of the algorithm is declared when the residuals $r(k)$, $s(k)$ in (21) are sufficiently small and the value $\max_{i,m} \{v_i^m l_i^m -$

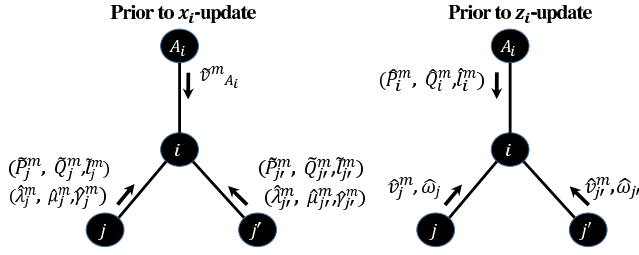


Fig. 2. Communication requirements of the ADMM algorithm. In each iteration, prior to the x -update, node i receives \hat{P}_j^m, \hat{Q}_j^m , and \hat{l}_j^m from its children nodes, and receives $\hat{v}_{A_i}^m$ from its ancestor node. Prior to the z -update, ancestor node A_i sends \hat{P}_i^m, \hat{Q}_i^m , and \hat{l}_i^m to node i while node i receives all the \hat{v}_j^m variables from its children. Note that whenever a variable is transmitted, its corresponding Lagrange multiplier is transmitted as well.

$(P_i^m)^2 - (Q_i^m)^2\}$ is smaller than 10^{-3} (pu) 2 . The latter ensures exactness of the SOCP relaxation in (7).

This section is wrapped up by highlighting the merits of the developed algorithm:

- 1) The algorithm comprises closed-form updates per node and per scenario. The need for solving complex optimization problems per node is therefore bypassed which greatly simplifies implementation.
- 2) Computational effort per node does not change as the size of the network increases—that is, each node still needs to run the same closed-form updates.
- 3) This distributed algorithm is conducive to maintaining user privacy. Specifically, global optimality is achieved while parameters such as bounds on user consumption (i.e., $p_{c_i}^{\min}, p_{c_i}^{\max}$), power factor, and user utility are not transmitted to a central agent.

Algorithm 1 Required Communications and Updates

- 1: Initialize z -variables and Lagrange multipliers with random numbers at every node i .
- 2: For every node i repeat steps 2-7 until convergence.
- 3: Receive $\hat{P}_j^m, \hat{Q}_j^m, \hat{l}_j^m, \hat{\lambda}_j^m, \hat{\mu}_j^m$, and $\hat{\gamma}_j^m$ from all $j \in C_i$ and for $m \in \mathcal{M}$. Also receive $\hat{v}_{A_i}^m$ from node A_i and $m \in \mathcal{M}$.
- 4: Perform x_i -update.
- 5: Receive the updated x -variables \hat{P}_i^m, \hat{Q}_i^m and \hat{l}_i^m for $m \in \mathcal{M}$ from A_i . Also receive \hat{v}_j^m and $\hat{\omega}_j^m$ from all nodes $j \in C_i$ and $m \in \mathcal{M}$.
- 6: Perform z_i -update.
- 7: Update the Lagrange multipliers.

VI. NUMERICAL TESTS

A. Network setup

Numerical simulations are conducted on a sample tree distribution network as illustrated in Fig. 3. Resistance and reactance values on line i , i.e., $r_i + jx_i$, are considered constant and equal to $0.33 + j0.38 \frac{\Omega}{\text{km}} \times d(\text{km})$ where d represents the distance between two nodes (fixed at 0.2km). For the network, $S_{\text{base}} = 1$ MVA is selected, while the substation voltage is fixed at $V_0 = 7.2$ kV. Voltage regulation is performed with $\epsilon =$

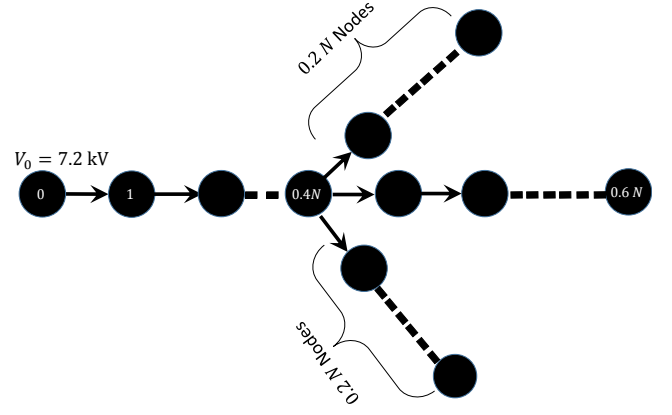


Fig. 3. Radial distribution network used in the numerical tests.

0.05 so that nodal voltages are allowed to vary within 5% of the nominal value V_0 . The line flow limit is $l_i^{\max} = 0.5(\text{kA})^2$. The cost $C(P_0^m)$ is set to zero, and similar to [38], the utility function is selected as $u_i(p_{c_i}) = -K_{u_i}(p_{c_i} - p_{c_i}^{\max})^2$. The objective weights are $K_{u_i} = 1$ and $K_{\text{Loss}} = 1$. Notice that if we set $K_{\text{Loss}} = 0$, then $C(P_0^m)$ can correctly account for loss terms.

For users $i = 1, \dots, N$, the non-elastic load is $P_{L_i} = 0.1$ MW, while p_{c_i} is constrained to be in $[0, p_{c_i}^{\max}] = [0, 0.05]$ MW. The power factor for both elastic and non-elastic loads is selected to be $\text{PF}_i = 0.94$.

B. Methodology for generating scenarios

If there is a PV unit at node i , then the relationship between s_{w_i} and the maximum real power capability of the inverter w_i^{\max} is given by $w_i^{\max} = \frac{s_{w_i}}{1.1}$. Following [35] and [36], the actual power generated by the PV unit, w_i , is a random variable that takes values from a beta distribution with mean \bar{w}_i and variance σ_i^2 , as follows:

$$f_{w_i}(w_i) = \frac{1}{w_i^{\max}} \left(\frac{w_i}{w_i^{\max}} \right)^{\alpha-1} \left(1 - \frac{w_i}{w_i^{\max}} \right)^{\beta-1} \quad (29a)$$

$$\text{Mean} = \bar{w}_i = \frac{\alpha}{\alpha + \beta} w_i^{\max} \quad (29b)$$

$$\text{Variance} = \sigma_i^2 = \frac{\alpha\beta}{(\alpha + \beta)^2(\alpha + \beta + 1)} (w_i^{\max})^2 \quad (29c)$$

where the relationship between the mean and the standard deviation is given as:

$$\frac{\sigma_i}{w_i^{\max}} = 0.2 \frac{\bar{w}_i}{w_i^{\max}} + 0.21. \quad (29d)$$

In each of the ensuing case studies, it is assumed that \bar{w}_i is known, and subsequently α and β can be found numerically using (29b) and (29c). Then, 1000 equiprobable scenarios are generated according to (29). This number is then reduced to $M = 7$ representative scenarios using the fast forward reduction method [5], [35].

The scenario reduction methodology starts with an original scenario set Ω with cardinality $|\Omega| = 1000$ and an empty set $\Omega_s = \emptyset$. Then, in each iteration, a scenario from $\Omega \setminus \Omega_s$ is selected which minimizes the Kantorovich Distance between Ω and Ω_s [5]. The algorithm stops once the prescribed

TABLE IV
OBJECTIVE VALUE BREAKDOWN FOR THE THREE DAY TYPES

Day Type Objective	Cloudy	Partly Cloudy	Sunny
Negative Utility $-\sum_{i=1}^N u_i(p_{c_i})$ monet. units	0.1142	0.0689	0.0232
Expected Thermal Losses $\sum_{m=1}^M \pi^m \sum_{i=1}^N r_i l_i^m$ (MW)	0.3181	0.0664	0.0271
Objective Value Total ($\times 10^6$)	0.4323	0.1357	0.0503

cardinality $|\Omega_s| = M = 7$ is achieved. The probability of scenarios that are not included in the reduced representative set (i.e., Ω_s) are aggregated on to the probability of the closest representative scenario in Ω_s . The choice for $M = 7$ is so that the smallest probability in the reduced set Ω_s is at least 0.01.

Remark (Number of scenarios in networks with N distributed generators). In a network with N generators whose power injections come from independent distributions, an exponential number of scenarios would potentially be needed to formulate the stochastic program. However, the stochastic program in this paper will not suffer from this exponential growth because of the following reasons: 1) Generators are all in a geographically limited area and under similar irradiance conditions, and hence generator outputs are spatially correlated; 2) the forecasted power output for the next time period—ranging from e.g., 15 minutes to 1 hour—is available, and is used to set the mean value of the distribution for each injection. The resulting distributions will have similar parameters, according to the type of day (e.g., sunny, cloudy, partly cloudy).

Different scenarios are generated for each of the case studies that follow, and problem (15) is solved. It is numerically verified for all problems that the SOCP inequality of (7) holds as equality for every scenario.

C. Case study for different day types

In this case study, the network features $N = 50$ nodes with 30 nodes on the main branch and two laterals of 10 nodes each branching off at node 20. Nodes 31 to 40 correspond to the first branch while nodes 41 to 50 correspond to the second branch. All users are equipped with distributed PV generators and one large PV generation unit is located at the terminal node of the main branch.

For the larger PV installation in the terminal node of the main branch, $s_{w_{30}} = 1$ MVA is selected, while for the remaining nodes we set $s_{w_i} = 0.1$ MVA. The ratio of $\frac{\bar{w}_i}{w_i^{\max}}$ takes the values 0.3, 0.6, and 0.9, corresponding respectively to cloudy, partly cloudy and sunny days.

Table IV shows the breakdown of objective values for problem (15) solved for the three different day types. As conditions range from cloudy to sunny, it is observed that the

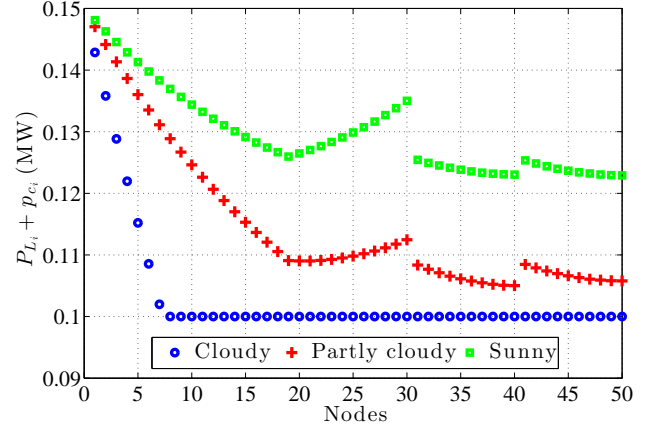


Fig. 4. Optimal user consumption values $P_{L_i} + p_{c_i}$ in three different day types. Level of satisfied demand increases as conditions range from cloudy to sunny.

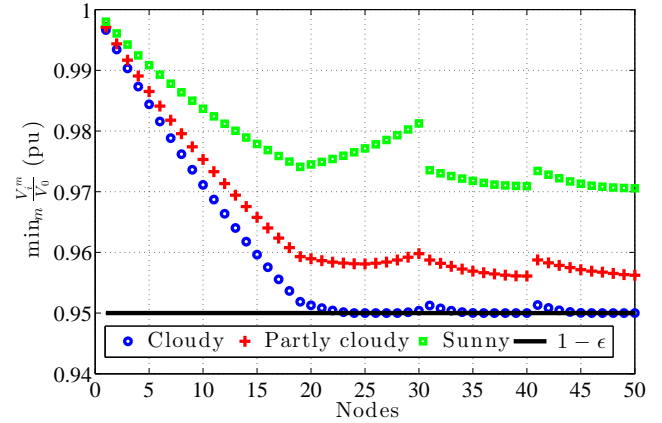


Fig. 5. Worst-case voltage profile across all scenarios for the three different day types. In a cloudy day, the voltage drop is high. As PV generation rises in partly cloudy and sunny days, voltage drops decrease.

level of satisfied elastic demand increases, while the expected thermal losses decrease. In particular, Fig. 4 shows the total load scheduled for each user in these three day types. On cloudy days, i.e., when PV generation is low, the proposed stochastic program ensures meeting the non-elastic demand. As PV generation increases during partly cloudy and sunny days, larger portions of the elastic demand are also guaranteed.

Fig. 5 depicts the worst-case voltage profile across all scenarios for the three different day types. There are three break points for each voltage plot. The voltage rise at node 30 corresponds to the larger generation of the terminal node. Voltage drop at node 20 corresponds to the branching of the network. On a cloudy day, the reduced power generation in the network results in a higher voltage drop. This voltage drop is smaller for improved solar conditions.

D. Comparison with distributed local control of [16]

The second set of numerical tests are conducted on a larger network with $N = 100$ nodes comprising 60 nodes on the main branch and two laterals each of length 20 branching off

at node 40. In this setup, 50% of the user nodes (randomly selected) are capable of PV generation. The terminal node on the main branch also provides large injection with $s_{w_{60}} = 1$ MVA, while $s_{w_i} = 0.4$ MVA is selected for the smaller generations. The simulations are performed for a sunny day. All other parameters are as listed in Subsections VI-A and VI-B.

In this case, problem (15) is solved first with $N = 100$, $M = 7$ scenarios and the optimal demand response schedules (i.e., p_{c_i} 's) are obtained. Then, in the online phase, problem (15) with p_{c_i} 's fixed to the previously found values is solved for a newly generated set of 100 scenarios. The results are compared to the ones obtained by the local reactive power control policy proposed in [16]. In this scheme, only the local variables w_i^m , p_{c_i} , and q_{c_i} , are used to set $q_{w_i}^m = F_i(w_i^m, P_{c_i}, Q_{c_i})$, where

$$F_i(w_i^m, P_{c_i}, Q_{c_i}) = \left[K F_i^{(L)} + (1 - K) F_i^{(V)} \right]_{-q_{w_i}^{\max}}^{q_{w_i}^{\max}} \quad (30)$$

$$F_i^{(L)} = [Q_{c_i}]_{-q_{w_i}^{\max}}^{q_{w_i}^{\max}} \quad (31)$$

$$F_i^{(V)} = \left[Q_{c_i} + \frac{x_i(P_{c_i} - w_i^m)}{r_i} \right]_{-q_{w_i}^{\max}}^{q_{w_i}^{\max}} \quad (32)$$

with $P_{c_i} = P_{L_i} + p_{c_i}$ and $Q_{c_i} = Q_{L_i} + q_{c_i}$.

This local control policy considers p_{c_i} and q_{c_i} to be specified and does not optimize the user consumption. Therefore, the optimal p_{c_i} and q_{c_i} values previously obtained by the solution of problem (15) are set as inputs to the local algorithm (30). Finally, upon setting $q_{w_i}^m$, the power flows P_i^m and Q_i^m as well as the voltages V_i^m can be found through solving the nonlinear power flow equations using Newton's method [39]. Notice that the parameter $K \in \mathbb{R}$ in (30) also needs to be experimentally set via trial and error.

Table V lists the thermal losses and the maximum voltage deviation resulting from the stochastic programming approach and the local control policy for different values of K .

The table reveals that for certain values of K (such as $K = 1.3$) the local control policy performs well in terms of thermal losses—partially due to the fact that the inputs to (30) are the optimal real power consumptions. However, the local control policy fails to guarantee that voltage levels are within the ϵ range. The best K in terms of voltage regulation was found with a grid search to be $K = 1.54$, resulting in a voltage deviation of 0.18 pu, which violates the voltage constraint, and in thermal losses of 0.18 MW—which is two times greater than that of the proposed stochastic programming approach.

To get a closer look at the voltage regulation, the empirical cumulative distribution function (CDF) of the maximum voltage deviation across nodes, i.e., $\max_i \frac{|V_i - V_0|}{V_0}$, is plotted in Fig. 6 for the stochastic programming approach as well as for different values of K . The CDF is obtained by counting the number of scenarios in the online phase for which $\max_i \frac{|V_i - V_0|}{V_0}$ is less than δV and dividing this number by the total number of 100 test scenarios. It is seen that the stochastic program, even by only considering just a few scenarios, guarantees the maximum voltage deviation to be less than the required threshold in all instances whereas the

TABLE V
OBJECTIVE VALUES, MAX VOLTAGE DEVIATION AND AVERAGE VOLTAGE DEVIATION

Method	Loss (MW)	$\max_{i,m} \frac{ V_i^m - V_0 }{V_0}$ (pu)
Stoch. Progr.	0.0940	0.0500
$K = 1.1$	0.1927	0.3682
$K = 1.2$	0.1229	0.3098
$K = 1.3$	0.1005	0.2647
$K = 1.4$	0.1155	0.2266
$K = 1.5$	0.1616	0.1931
$K = 1.6$	0.2341	0.2018
$K = 1.7$	0.2674	0.2154
$K = 1.8$	0.2622	0.2166
$K = 1.9$	0.2539	0.2166
$K = 3$	0.2440	0.2160

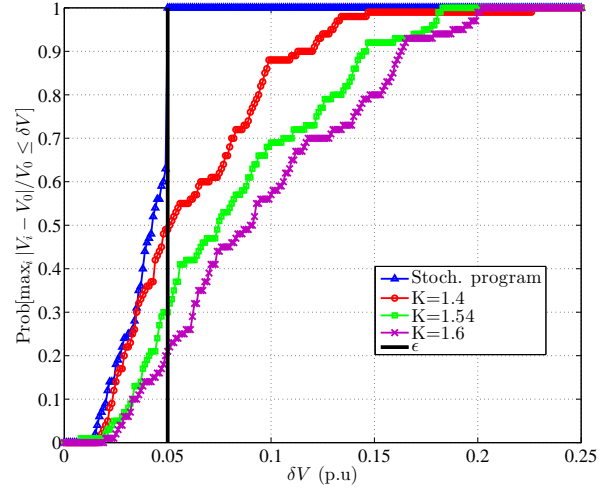


Fig. 6. Empirical cumulative distribution function of the maximum voltage deviation, i.e., $\max_i \frac{|V_i - V_0|}{V_0}$, for the proposed stochastic model as well as local control policy with several values of K . Ideally, it is preferred to have the CDF plots to be on the left side of the solid ϵ line which corresponds to voltage deviations below ϵ .

CDF induced by the local control policy reveals that voltage deviations may exceed the required threshold.

E. Case study on a feeder with shunt capacitors

To show effectiveness of inverter reactive power control, the 56-node network of [19, Fig. 2] that already includes shunt capacitors is selected for additional numerical tests. The details of the network are given in [19, Table I]. Only non-elastic load is considered in this case study (i.e., $p_{c_i} = 0$). The values for P_{L_i} 's and Q_{L_i} 's are calculated using the apparent peak load in [19, Table I] increased by 50 % because the original network is

TABLE VI
NUMBER OF INFEASIBLE SCENARIOS WHEN REACTIVE POWER
COMPENSATION OF PV INVERTERS IS NOT ALLOWED

PV Penetration (%)	30	55	60	65	70
No. Infeasible cases	100	92	61	29	8

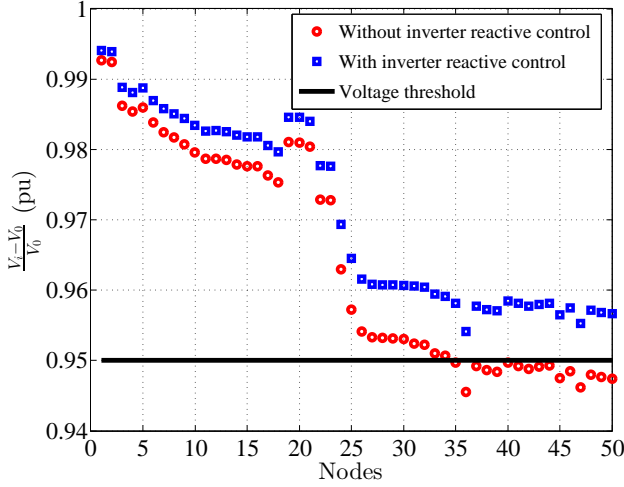


Fig. 7. Voltage profile $\frac{|V_i - V_0|}{V_0}$ for a fixed scenario. When inverters do not provide reactive power compensation, the voltage drop may exceed the threshold; while allowing reactive power compensation can prevent this drop.

lightly loaded, and assuming $\text{PF}_i = 0.94$ per node. All nodes are PV-enabled. By defining PV penetration level as the ratio of total PV apparent power capability to the total load, s_{w_i} 's per node are varied so that different PV penetration levels can be simulated.

Problem (12) is first solved for 100 PV generation scenarios when reactive power compensation by PV inverters is not allowed (i.e., $q_{w_i}^m = 0$). The number of infeasible scenarios is recorded in Table VI. For the same scenarios, problem (12) is solved with reactive power compensation capability as in (3). In this case, all scenarios were feasible.

When inverters are not allowed to compensate for reactive power, voltages may drop below the required threshold, while reactive power provided by the inverters prevents large voltage drops and increases system reliability. The voltage profile for a scenario with $w_i = \bar{w}_i$ and $\sum_i \bar{w}_i = 0.5 \sum_i P_{L_i}$ (i.e., 50 % penetration) is also plotted in Fig. 7 to illustrate this effect.

F. Effect of stepsize ρ in convergence of ADMM

This subsection numerically investigates the effect of the stepsize ρ on the convergence of the ADMM algorithm. In particular, the network setup in Subsection VI-A is considered here, where 50% of nodes are capable of PV generation with $s_{w_i} = 0.15$ MVA, and $s_{w_{50}} = 1.5$ MVA for the terminal node at one of the laterals. Moreover, $\frac{\bar{w}_i}{w_i^{\max}} = 0.75$ is selected. The remaining parameters are selected as described in Subsections VI-A and VI-B. Initially, 1000 scenarios are generated, which are subsequently reduced to $M = 7$ scenarios. Problem (15) is then solved using the ADMM algorithm of Section IV for three

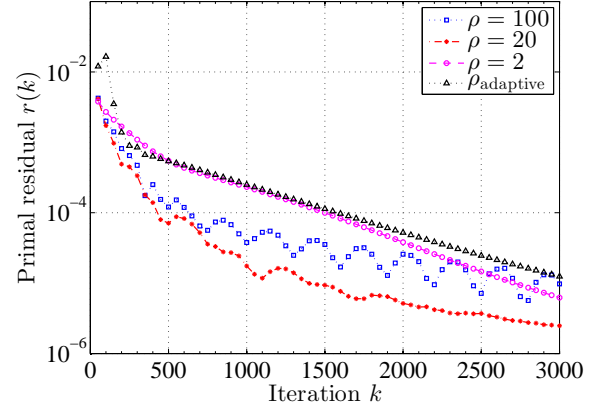


Fig. 8. Primal residual per ADMM iteration for various stepsizes ($\rho = 2, 20, 100$ and ρ_{adaptive}).

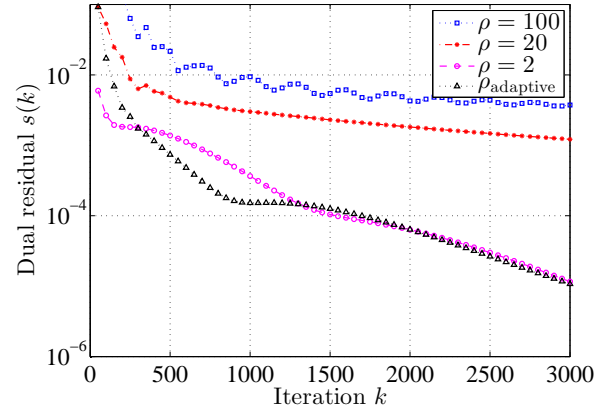


Fig. 9. Dual residual per ADMM iteration for various stepsizes ($\rho = 2, 20, 100$ and ρ_{adaptive}).

constant stepsizes, namely $\rho = 2, 20, 100$, and one adaptive stepsize (ρ_{adaptive}) according to the following rule [37]:

$$\rho(k+1) := \begin{cases} 2\rho(k) & \text{if } \|r(k)\| > 10\|s(k)\| \\ \frac{\rho(k)}{2} & \text{if } \|s(k)\| > 10\|r(k)\| \\ \rho(k) & \text{otherwise} \end{cases} \quad (33)$$

where $\rho(1) = 100$, and the primal and dual residuals, i.e., $r(k)$ and $s(k)$, are respectively calculated via (21a) and (21b).

The resulting primal and dual residuals per iteration are respectively given in Fig. 8 and 9 for the various values of ρ . All choices of ρ (including the adaptive one) perform well in terms of reducing the primal residual, while $\rho = 20$ and $\rho = 100$ perform poorly in minimizing the dual residual [potentially due to the multiplication in (21b)]. Moreover, $\rho = 2$ and ρ_{adaptive} have a similar performance, noting that the ρ_{adaptive} reaches 1.56 upon convergence.

The objective value per iteration is shown in Fig. 10 for the various values of ρ . For $\rho = 100$, an accurate objective value is not found within the 3000 iterations. The exactness of the SOCP relaxation, i.e., $\max_{i,m} |(P_i^m)^2 + (Q_i^m)^2 - v_i^m l_i^m|$, is depicted in Fig. 11. This value eventually approaches zero for all values of ρ ; however, the progress is rather slow after 1000 iterations in the case of $\rho = 2$ or ρ_{adaptive} .

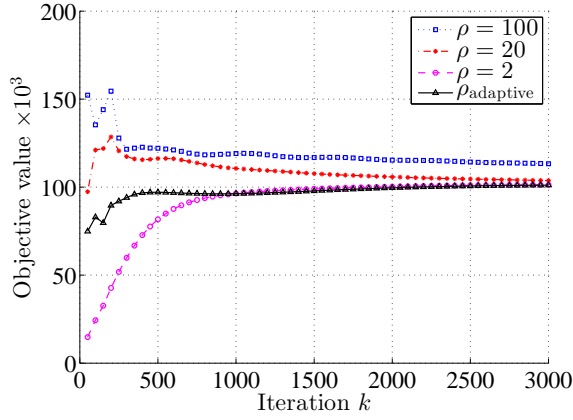


Fig. 10. Comparison of objective value per ADMM iteration for various stepsizes ($\rho = 2, 20, 100$ and ρ_{adaptive}).

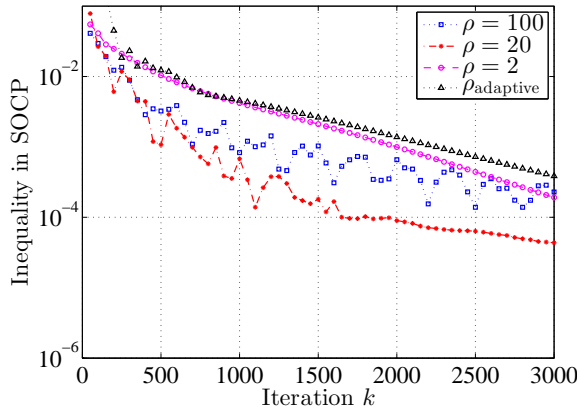


Fig. 11. Exactness of the SOCP relaxation, i.e., $\max_{i,m} |(P_i^m)^2 + (Q_i^m)^2 - v_i^m l_i^m|$, per ADMM iteration for various stepsizes ($\rho = 2, 20, 100$ and ρ_{adaptive}).

G. Effect of number of scenarios on convergence

This section investigates the convergence of ADMM under larger number of scenarios. Problem (15) is solved for the network of Fig. 3. The penetration level is set to 50%, while $s_{w_i} = 0.15$ (MVA) is selected for PV-enabled nodes, and $s_{w_{50}} = 1.5$ (MVA) is chosen for the terminal node at one lateral. Problem (15) is solved using $M = 100$ and $M = 500$ randomly generated equiprobable scenarios with $\frac{\bar{w}_i}{w_i^{\max}} = 0.75$. Table VII lists the parameters indicating the convergence in these two test cases. The algorithm scalability is not necessarily dependent on the number of scenarios, but rather on the network structure and the specific power injections per node. As long as each node is capable of performing individual updates for the specified number of scenarios, the algorithm will converge.

VII. CONCLUSION

This paper developed a stochastic power management framework for radial distribution networks with high levels of PV penetration. Decision variables included real power consumption of programmable loads in user nodes and the reactive power generation or consumption of the PV inverters. The uncertain real power injections of the user buses were

TABLE VII
CONVERGENCE OF ADMM FOR INCREASED NUMBER OF SCENARIOS

M	100	500
Number of iterations	3059	4100
Primal residual $r(k)$	9.9×10^{-6}	2.23×10^{-5}
Dual residual $s(k)$	1.24×10^{-6}	4.4×10^{-5}
$\max_{i,m} (P_i^m)^2 + (Q_i^m)^2 - v_i^m l_i^m $	8.24×10^{-4}	9.38×10^{-4}

modeled as random variables taking values from a finite number of scenarios. A convex stochastic optimization program was formulated to minimize the sum of negative utility, the expected value of cost of power provision, and the expected thermal losses subject to the SOCP relaxation of the power flow equations, power consumption constraints, and voltage regulation specifications. A decentralized method using the ADMM was developed to solve the stochastic program, in which the updates per node and per scenario turn out to be in closed form.

APPENDIX A

PROOF THAT AT MOST ONE OF THE TWO VARIABLES P_{0+}^m AND P_{0-}^m IS NONZERO

Let \tilde{P}_{0+}^m and \tilde{P}_{0-}^m be the solution of (12) with $C(P_0^m)$ replaced by $aP_{0+}^m - bP_{0-}^m$. Suppose that $\tilde{P}_{0+}^m > 0$ and $\tilde{P}_{0-}^m > 0$. Then, $\tilde{P}_{0+}^m - \epsilon$ and $\tilde{P}_{0-}^m - \epsilon$ are feasible for sufficiently small $\epsilon > 0$ and give an objective $a\tilde{P}_{0+}^m - b\tilde{P}_{0-}^m - (a - b)\epsilon$ which is strictly smaller than $a\tilde{P}_{0+}^m - b\tilde{P}_{0-}^m$ since $a > b$. This is a contradiction.

APPENDIX B

ON THE EXACTNESS OF THE SOCP RELAXATION

Based on [14], this appendix presents conditions under which the optimal solution to problem (12) satisfies (7) with equality. In order to state the results, some notations are introduced next.

Given net nodal consumptions $(P_{L_i} + p_{c_i} - w_i^m, Q_{L_i} + q_{c_i} - q_{w_i}^m)$, the solution to the LinDistFlow approximation of the power flow equations presented in (4)–(6) for scenario m is given by:

$$\check{P}_i^m(\mathbf{p}_c) = \sum_{j:i \in \mathcal{P}_j} (P_{L_j} + p_{c_j} - w_j^m) \quad (34)$$

$$\check{Q}_i^m(\mathbf{p}_c, \mathbf{q}_w^m) = \sum_{j:i \in \mathcal{P}_j} (Q_{L_j} + q_{c_j} - q_{w_j}^m) \quad (35)$$

$$\check{v}_i^m(\mathbf{p}_c, \mathbf{q}_w^m) = v_0 - 2 \sum_{j \in \mathcal{P}_i^+} [r_j \check{P}_j^m + x_j \check{Q}_j^m] \quad (36)$$

where $q_{c_j} = \left(\sqrt{\frac{1}{\text{PF}_j^2} - 1} \right) p_{c_j}$, \mathcal{P}_j is the unique path from the root node to node j (including node j), and \mathcal{P}_j^+ is $\mathcal{P}_j \setminus \{0\}$. Also, \mathbf{p}_c and \mathbf{q}_w^m collect the corresponding values of all nodes.

Now, consider the following modifications of problem (12):

- 1) Assume $C(P_0^m)$ to be strictly increasing in P_0^m ;
- 2) remove the upper bounds on the current magnitudes;
- 3) consider shunt capacitors to be modeled by fixed reactive power injections and independent of voltage magnitudes;

- 4) set $K_{\text{Loss}} = 0$; and
- 5) enforce the constraint $\check{v}_i^m(p_{c_i}, q_{w_i}^m) \leq (1 + \epsilon)^2 v_0$, instead of $v_i^m \leq (1 + \epsilon)^2 v_0$.

In addition, following [14], define for every scenario m ,

$$\underline{A}_i^m := I + \frac{2}{(1 - \epsilon)^2 v_0} \begin{bmatrix} r_i \\ x_i \end{bmatrix} [\check{P}_i^{m-}(\mathbf{p}_c^{\min}) \quad \check{Q}_i^{m-}(\mathbf{p}_c^{\min}, \mathbf{s}_w)]$$

where $a^- = \min\{a, 0\}$. Also \mathbf{p}_c^{\min} and \mathbf{s}_w collect all the corresponding values per node. Then, the main result is that the modified SOCP problem is exact if the following condition holds for every scenario m :

$$\prod_{j=s+1}^{t-1} \underline{A}_{d_j}^m \begin{bmatrix} r_{d_t} \\ x_{d_t} \end{bmatrix} > 0, \text{ for } 2 \leq t \leq n_d, 0 \leq s \leq t-2 \quad (37)$$

where $n_d = |\mathcal{P}_i|$ for all leaf nodes i (i.e., nodes such that $\mathcal{C}_i = \emptyset$) and $d_j \in \mathcal{P}_i$.

A sketch of proof based on [14] is presented next. For given p_{c_i} and $q_{w_i}^m$, we can establish that if P_i^m , Q_i^m and v_i^m satisfy (4)–(6), then the following holds (equivalent to [14, Lemma 1]):

$$\check{P}_i^m(\mathbf{p}_c) \leq P_i^m \quad (38)$$

$$\check{Q}_i^m(\mathbf{p}_c, \mathbf{q}_w^m) \leq Q_i^m \quad (39)$$

$$\check{v}_i^m(\mathbf{p}_c, \mathbf{q}_w^m) \geq v_i^m. \quad (40)$$

Assume we solve problem (12) and it turns out that (7) is not satisfied with equality in at least one node and one scenario. Here we show that we can construct a feasible solution with a lower objective value. Call that scenario m and label the node K . Further, without loss of generality, we can assume that the node K is the $k+1$ 'th node in \mathcal{P}_{d_n} where d_n is a leaf node and $|\mathcal{P}_{d_n}| = n+1$. Path \mathcal{P}_{d_n} is illustrated as follows:

$$0 \xrightarrow{1} d_1 \xrightarrow{2} d_2 \dots \xrightarrow{k} d_k = K \xrightarrow{k+1} \dots \xrightarrow{n} d_n. \quad (41)$$

The current solution will be called $s = (\mathbf{P}, \mathbf{Q}, \mathbf{v}, \mathbf{l}, \mathbf{p}_c, \mathbf{q}_w)$, where $\mathbf{P}, \mathbf{Q}, \mathbf{v}, \mathbf{l}, \mathbf{p}_c, \mathbf{q}_w$ are vectors collecting all the corresponding values per node and per scenario. Solution s has the the following property:

$$\frac{(P_K^m)^2 + (Q_K^m)^2}{v_K^m} < l_K^m, \quad (42)$$

$$\frac{(P_{d_i}^m)^2 + (Q_{d_i}^m)^2}{v_{d_i}^m} = l_{d_i}^m \quad \text{for } i = 1, \dots, k-1. \quad (43)$$

Algorithm 2 constructs a new feasible solution $s' = (\mathbf{P}', \mathbf{Q}', \mathbf{v}', \mathbf{l}', \mathbf{p}_c', \mathbf{q}_w')$, which will be proved to have a lower objective. In particular, the new solution s' has the following properties:

$$l_K^m < l_K^m \Rightarrow \Delta l_K^m = l_K^m - l_K^m < 0, \quad (44)$$

$$\frac{(P_i^m)^2 + (Q_i^m)^2}{v_i^m} \leq l_i^m \quad \text{for all } i \in \mathcal{N} \setminus \{0\}. \quad (45)$$

At this point, by proving that $v_i^m \geq v_i^m$, we can use (45) to show that s' is feasible. Furthermore, by additionally proving that $P_0^m < P_0^m$, the new solution will have a smaller objective value, which yields a contradiction. These two facts are proved next.

Algorithm 2 Constructing s' from s with lower objective

1: Initialization: $s' \leftarrow s$, $v_0' \leftarrow v_0$, $\mathcal{N}_{\text{visit}} = \{0\}$.

2: Backward sweep: **For** $i = k, \dots, 1$ **do**

$$l_{d_i}^m \leftarrow \frac{(P_{d_i}^m)^2 + (Q_{d_i}^m)^2}{v_{d_i}^m} \quad (46)$$

$$P_{d_{i-1}}^m \leftarrow \sum_{j \in \mathcal{C}_{d_{i-1}}} P_j^m + r_j l_j^m + P_{L_{d_i}}^m + p_{c_{d_i}}' - w_{d_i}^m \quad (47)$$

$$Q_{d_{i-1}}^m \leftarrow \sum_{j \in \mathcal{C}_{d_{i-1}}} Q_j^m + x_j l_j^m + Q_{L_{d_i}}^m + \left(\sqrt{\frac{1}{\text{PF}_{d_i}^2} - 1} \right) p_{c_{d_i}}' - q_{w_{d_i}}^m. \quad (48)$$

3: Forward sweep: **While** $\mathcal{N}_{\text{visit}} \neq \mathcal{N}$ **do**

$$\text{find } j \notin \mathcal{N}_{\text{visit}}, i \in \mathcal{N}_{\text{visit}} \text{ such that } j \in \mathcal{C}_i, \quad (49)$$

$$v_j^m = v_i^m - 2r_i P_j^m - 2x_i Q_j^m - (r_i^2 + x_i^2) l_j^m, \quad (50)$$

$$\mathcal{N}_{\text{visit}} \leftarrow \mathcal{N}_{\text{visit}} \cup \{j\}. \quad (51)$$

Define $\Delta P_i^m = P_i^m - P_i^m$ and $\Delta Q_i^m = Q_i^m - Q_i^m$. We can establish the following on path \mathcal{P}_{d_k} :

$$\begin{bmatrix} \Delta P_{d_{i-1}}^m \\ \Delta Q_{d_{i-1}}^m \end{bmatrix} = B_{d_i}^m \begin{bmatrix} \Delta P_{d_i}^m \\ \Delta Q_{d_i}^m \end{bmatrix} \quad (52)$$

where for $i = k, \dots, 1$:

$$B_{d_i}^m = \left(I + \frac{2}{v_{d_i}^m} \begin{bmatrix} r_{d_i} \\ x_{d_i} \end{bmatrix} \begin{bmatrix} \frac{P_{d_i}^m + P_{d_i}^m}{2} & \frac{Q_{d_i}^m + Q_{d_i}^m}{2} \end{bmatrix} \right) \quad (53)$$

and

$$\begin{bmatrix} \Delta P_{d_k}^m \\ \Delta Q_{d_k}^m \end{bmatrix} = \begin{bmatrix} r_{d_k} \\ x_{d_k} \end{bmatrix} \Delta l_K^m. \quad (54)$$

Thus we can write for $s = k-2, \dots, 0$

$$\begin{bmatrix} \Delta P_{d_s}^m \\ \Delta Q_{d_s}^m \end{bmatrix} = \prod_{i=s+1}^{k-1} B_{d_i}^m \begin{bmatrix} r_{d_k} \\ x_{d_k} \end{bmatrix} \Delta l_K^m. \quad (55)$$

Observe that $B_{d_i}^m - \underline{A}_{d_i}^m = \begin{bmatrix} r_{d_i} \\ x_{d_i} \end{bmatrix} b_{d_i}^T$, where

$$b_{d_i} = \begin{bmatrix} \frac{P_{d_i}^m + P_{d_i}^m}{2v_{d_i}^m} - \frac{\check{P}_{d_i}^{m-}(\mathbf{p}_c^{\min})}{(1-\epsilon)^2 v_0} \\ \frac{Q_{d_i}^m + Q_{d_i}^m}{2v_{d_i}^m} - \frac{\check{Q}_{d_i}^{m-}(\mathbf{p}_c^{\min}, \mathbf{s}_w)}{(1-\epsilon)^2 v_0} \end{bmatrix} \geq 0, \quad (56)$$

for $i = k-1, \dots, 1$. Therefore, [14, Lemma 3] can be used to show that $P_{d_i}^m < P_{d_i}^m$ and $Q_{d_i}^m < Q_{d_i}^m$ for $i = k-1, \dots, 0$. Notice that $d_0 = 0$ and hence the following holds:

$$P_0^m < P_0^m. \quad (57)$$

Next, we show that $v_i^m \geq v_i^m$. Define $\Delta v_i^m = v_i^m - v_i^m$. For $A_i \notin \mathcal{P}_K$, we have that

$$\Delta v_i^m - \Delta v_{A_i}^m = -2r_i \Delta P_i^m - 2x_i \Delta Q_i^m - (r_i^2 + x_i^2) \Delta l_i^m = 0. \quad (58)$$

For $A_i \in \mathcal{P}_K$, it holds that

$$\Delta v_i^m - \Delta v_{A_i}^m = -2r_i \Delta P_i^m - 2x_i \Delta Q_i^m - (r_i^2 + x_i^2) \Delta l_i^m \geq 0. \quad (59)$$

Adding these inequalities over path \mathcal{P}_{d_k} yields

$$\Delta v_i^m - \Delta v_0 \geq 0 \Rightarrow \Delta v_i^m \geq 0, \text{ for } i \in \mathcal{P}_{d_k}, \quad (60)$$

which proves that $v_i'^m \geq v_i^m$. We have shown that solution s' is feasible. Due to (57) and the assumption that $C(P_0)$ is strictly increasing, the new solution s' has a smaller objective; this is a contradiction.

We have derived sufficient condition (37) under which the SOCP relaxation is exact for a modified problem close to problem (12). This sufficient condition can be checked a priori. Notice that modifications 1–3 and 5 are exactly the same as the ones proposed in [14] where the problem is not stochastic.

Condition (37) is stated per scenario. It is also possible to state a single sufficient condition that does not depend on m . Specifically, replace w_i^m 's with $\max_m w_i^m$ in (34); then, the resulting matrix \underline{A}_i does not depend on m , and condition (37) is stated with \underline{A}_i instead of \underline{A}_i^m . This latter condition is a more stringent sufficient condition that accounts for the lowest-consumptions. We have numerically verified that this latter sufficient condition holds for the network in the numerical tests.

APPENDIX C

CLOSED-FORM UPDATES FOR $\tilde{P}_i^m, \tilde{Q}_i^m, \tilde{v}_i^m, \tilde{l}_i^m$

Let $z_1 = \tilde{P}_i^m$, $z_2 = \tilde{Q}_i^m$, $z_3 = \sqrt{\frac{|C_i|+1}{2}} \tilde{v}_i^m$ and $z_4 = \tilde{l}_i^m$. The z-update for these variables will be equivalent to solving the following optimization problem:

$$\min_{z_1, z_2, z_3, z_4} \sum_{i=1}^4 (z_i^2 + c_i z_i) \quad (61a)$$

$$\text{subject to} \quad (61b)$$

$$z_3^{\min} \leq z_3 \leq z_3^{\max} \quad (61c)$$

$$\frac{z_1^2 + z_2^2}{z_3} \leq k^2 z_4 \quad (61d)$$

$$z_4 \leq z_4^{\max} \quad (61e)$$

where

$$\begin{aligned} k^2 &= \sqrt{\frac{2}{|C_i|+1}} \\ z_3^{\max} &= \sqrt{\frac{|C_i|+1}{2}} (1+\epsilon)^2 v_0 \\ z_3^{\min} &= \sqrt{\frac{|C_i|+1}{2}} (1-\epsilon)^2 v_0 \\ c_1 &= -(P_i^m + \hat{P}_i^m + \frac{\lambda_i^m + \hat{\lambda}_i^m}{\rho}) \\ c_2 &= -(Q_i^m + \hat{Q}_i^m + \frac{\mu_i^m + \hat{\mu}_i^m}{\rho}) \\ c_3 &= -(v_i^m + \sum_{j \in \mathcal{C}_i} \hat{v}_j^m + \frac{\gamma_i^m + \hat{\gamma}_i^m}{\rho}) \\ c_4 &= -(l_i^m + \hat{l}_i^m + \frac{\gamma_i^m + \hat{\gamma}_i^m}{\rho}). \end{aligned}$$

Problem (61) without considering constraint (61e) is solved in closed-form in [22, Appendix I]. Using a similar approach, we develop a methodology to obtain a closed-form solution to problem (61), when it includes constraint (61e).

Let $\bar{\lambda}, \underline{\lambda}, \mu$ and $\gamma \geq 0$ be Lagrange multipliers corresponding to (61c), (61d) and (61e) respectively. The KKT conditions for problem (61) are:

$$2z_1 + c_1 + 2\mu \frac{z_1}{z_3} = 0 \quad (62a)$$

$$2z_2 + c_2 + 2\mu \frac{z_2}{z_3} = 0 \quad (62b)$$

$$2z_3 + c_3 - \mu \frac{z_1^2 + z_2^2}{z_3^2} + \bar{\lambda} - \underline{\lambda} = 0 \quad (62c)$$

$$2z_4 + c_4 - k^2 \mu + \gamma = 0 \quad (62d)$$

$$\bar{\lambda}(z_3 - z_3^{\max}) = 0 \quad (62e)$$

$$\underline{\lambda}(z_3^{\min} - z_3) = 0 \quad (62f)$$

$$\mu \left(\frac{z_1^2 + z_2^2}{z_3} - k^2 z_4 \right) = 0 \quad (62g)$$

$$\gamma(z_4 - z_4^{\max}) = 0. \quad (62h)$$

The closed-form solution for the KKT conditions in (62) is obtained by enumerating the cases for γ :

A. Case 1: $\gamma = 0$

In this case, as detailed in [22, Appendix I], there exists a unique solution to (62) which can be obtained in closed form. If the obtained closed-form solution satisfies $z_4 \leq z_4^{\max}$ then it is also optimal for (61). Otherwise, we need to proceed to the next case.

B. Case 2: $\gamma > 0$

In this case, using (62h), we can establish that $z_4^* = z_4^{\max}$. Now we examine possible choices for μ .

1) $\mu = 0$:

$$z_1^* = -\frac{c_1}{2}, z_2^* = -\frac{c_2}{2}, z_3^* = -\left[\frac{c_3}{2}\right]_{z_3^{\min}}^{z_3^{\max}}.$$

2) $\mu > 0$, $z_3^{\min} < z_3 < z_3^{\max}$:

$$z_3^* = \text{solve}(az_3^2 + bz_3 + c = 0)$$

where

$$a = k^2 z_4^{\max} \left(2 + \frac{4}{z_4^{\max}}\right)^2$$

$$b = \frac{4}{z_4^{\max}} c_3 \left(2 + \frac{4}{z_4^{\max}}\right) k^2 z_4^{\max} - (c_1^2 + c_2^2)$$

$$c = \frac{4k^2}{z_4^{\max}} c_3^2$$

$$z_1^* = -\frac{c_1 z_3^*}{2z_3^* + \frac{4}{z_4^{\max}} z_3^* + \frac{2}{z_4^{\max}} c_3}$$

$$z_2^* = \frac{c_2}{c_1} z_1^*.$$

$$3) \mu > 0, z_3^{\min} = z_3:$$

$$\begin{aligned} z_3^* &= z_3^{\min} \\ z_1^* &= -\frac{c_1 z_3^*}{2\mu^* + 2z_3^*} \\ z_2^* &= -\frac{c_2}{c_1} z_1^* \\ \mu^* &= \frac{\sqrt{c_1^2 + c_2^2} \sqrt{z_3^{\min}}}{2\sqrt{k^2 z_4^{\max}}} - z_3^{\min}. \end{aligned}$$

$$4) \mu > 0, z_3^{\max} = z_3:$$

$$\begin{aligned} z_3^* &= z_3^{\max} \\ z_1^* &= -\frac{c_1 z_3^*}{2\mu^* + 2z_3^*} \\ z_2^* &= -\frac{c_2}{c_1} z_1^* \\ \mu^* &= \frac{\sqrt{c_1^2 + c_2^2} \sqrt{z_3^{\max}}}{2\sqrt{k^2 z_4^{\max}}} - z_3^{\max}. \end{aligned}$$

REFERENCES

- [1] "IEEE 1547 standard for interconnecting distributed resources with electric power systems." [Online]. Available: <http://ieeexplore.ieee.org/stamp/stamp.jsp?arnumber=1225051>
- [2] K. Turitsyn, P. Šulc, S. Backhaus, and M. Chertkov, "Options for control of reactive power by distributed photovoltaic generators," *Proc. of the IEEE*, vol. 99, no. 1, pp. 1063–1073, June 2011.
- [3] M. E. Baran and I. M. El-Markabi, "A multiagent-based dispatching scheme for distributed generators for voltage support on distribution feeders," *IEEE Trans. Power Syst.*, vol. 22, no. 1, pp. 52–59, Feb. 2007.
- [4] D. Villacci, G. Bontempi, and A. Vaccaro, "An adaptive local learning-based methodology for voltage regulation in distribution networks with dispersed generation," *IEEE Trans. Power Syst.*, vol. 21, no. 3, pp. 1131–1140, Aug. 2006.
- [5] A. J. Conejo, M. Carrion, and J. M. Morales, *Decision making under uncertainty in electricity markets*. New York: Springer, 2010.
- [6] M. E. Baran and F. F. Wu, "Optimal sizing of capacitors placed on a radial distribution feeder," *IEEE Trans. Power Del.*, vol. 4, no. 1, pp. 735–743, Jan. 1989.
- [7] —, "Optimal capacitor placement on radial distribution systems," *IEEE Trans. Power Del.*, vol. 4, no. 1, pp. 725–734, Jan. 1989.
- [8] —, "Network reconfiguration in distribution systems for loss reduction and load balancing," *IEEE Trans. Power Del.*, vol. 4, no. 2, pp. 1401–1407, Apr. 1989.
- [9] S. H. Low, "Convex relaxation of optimal power flow—part II: Exactness," *IEEE Trans. Control of Netw. Syst.*, vol. 1, no. 2, pp. 177–189, June 2014.
- [10] —, "Convex relaxation of optimal power flow—part I: Formulations and equivalence," *IEEE Trans. Control of Netw. Syst.*, vol. 1, pp. 15–27, Mar. 2014.
- [11] R. A. Jabr, "Radial distribution load flow using conic programming," *IEEE Trans. Power Syst.*, vol. 21, no. 3, pp. 1458–1459, Aug. 2006.
- [12] J. Lavaei and S. H. Low, "Zero duality gap in optimal power flow problem," *IEEE Trans. Power Syst.*, vol. 27, no. 1, pp. 92–107, Feb. 2012.
- [13] S. Sojoudi and J. Lavaei, "Physics of power networks makes hard optimization problems easy to solve," in *Proc. PES General Meeting*, San Diego, CA, USA, July 2012, pp. 1–8.
- [14] L. Gan, N. Li, U. Topcu, and S. H. Low, "Exact convex relaxation of optimal power flow in radial networks," *IEEE Trans. Autom. Control*, vol. 60, no. 1, pp. 72–87, Jan. 2015.
- [15] K. Turitsyn, P. Šulc, S. Backhaus, and M. Chertkov, "Distributed control of reactive power flow in a radial distribution circuit with high photovoltaic penetration," in *Proc. IEEE PES General Meeting*, Minneapolis, MN, July 2010, pp. 1–6.
- [16] —, "Local control of reactive power by distributed photovoltaic generators," in *Proc. IEEE Int. Conf. Smart Grid Communications*, Oct. 2010, pp. 79–84.
- [17] P. Šulc, S. Backhaus, and M. Chertkov, "Optimal distributed control of reactive power via the alternating direction method of multipliers," *IEEE Trans. Energy Convers.*, vol. 29, no. 4, pp. 968–977, Dec. 2014.
- [18] H. Yeh, D. F. Gayme, and S. H. Low, "Adaptive VAR control for distribution circuits with photovoltaic generators," *IEEE Trans. Power Systems*, vol. 27, no. 3, pp. 1656–1663, Aug. 2012.
- [19] M. Farivar, R. Neal, C. Clarke, and S. Low, "Optimal inverter VAR control in distribution systems with high PV penetration," in *Proc. IEEE PES General Meeting*, San Diego, CA, July 2012, pp. 1–7.
- [20] N. Li, L. Gan, L. Chen, and S. H. Low, "An optimization-based demand response in radial distribution networks," in *Proc. IEEE Workshop Smart Grid Communications: Design for Performance*, Anaheim, CA, Dec. 2012, pp. 1–6.
- [21] N. Li, L. Chen, and S. H. Low, "Demand response in radial distribution networks: Distributed algorithm," in *Proc. Asilomar Conf. Signals, Systems, and Computers*, Pacific Grove, CA, Nov. 2012, pp. 1549–1553.
- [22] Q. Peng and S. H. Low, "Distributed algorithm for optimal power flow on a radial network," *arxiv*, May. 2015. [Online]. Available: <http://arxiv.org/pdf/1404.0700v2.pdf>
- [23] M. Kraning, E. Chu, J. Lavaei, and S. Boyd, "Dynamic network energy management via proximal message passing," *Foundations and Trends in Optimization*, vol. 1, no. 2, pp. 1–54, 2013.
- [24] E. Dall'Anese, H. Zhu, and G. B. Giannakis, "Distributed optimal power flow for smart microgrids," *IEEE Trans. Smart Grid*, vol. 4, no. 3, pp. 1464–1475, Sept. 2013.
- [25] E. Dall'Anese, S. Dhople, B. Johnson, and G. B. Giannakis, "Decentralized optimal dispatch of photovoltaic inverters in residential distribution systems," *IEEE Trans. Energy Convers.*, vol. 29, no. 4, pp. 957–967, Dec. 2014.
- [26] A. Lam, B. Zhang, A. Dominguez-Garcia, and D. Tse, "Optimal distributed voltage regulation in power distribution networks," *arxiv*, Apr. 2012. [Online]. Available: <http://arxiv.org/pdf/1204.5226v3.pdf>
- [27] B. A. Robbins, C. N. Hadjicostis, and A. D. Domínguez-García, "A two-stage distributed architecture for voltage control in power distribution systems," *IEEE Trans. Power Syst.*, vol. 28, no. 2, pp. 1470–1482, May 2013.
- [28] S. Deshmukh, B. Natarajan, and A. Pahwa, "Voltage/var control in distribution networks via reactive power injection through distributed generators," *IEEE Trans. Smart Grid*, vol. 3, no. 3, pp. 1226–1234, Sept. 2012.
- [29] S. Bolognani, R. Carli, G. Cavraro, and S. Zampieri, "A distributed control strategy for optimal reactive power flow with power and voltage constraints," in *Proc. 52nd IEEE Conf. Decision and Control*, Firenze, Oct. 2013, pp. 115–120.
- [30] —, "Distributed reactive power feedback control for voltage regulation and loss minimization," *IEEE Trans. Autom. Control*, vol. 60, no. 4, Apr. 2015.
- [31] N. Li, G. Qu, and M. Dahleh, "Real-time decentralized voltage control in distribution networks," in *Communication, Control, and Computing (Allerton)*, 2014 52nd Annual Allerton Conference on, Sept 2014, pp. 582–588.
- [32] V. Kekatos, G. Wang, A. Conejo, and G. Giannakis, "Stochastic reactive power management in microgrids with renewables," *IEEE Trans. Power Syst.*, accepted. [Online]. Available: <http://arxiv.org/pdf/1409.6758.pdf>
- [33] E. Dall'Anese, S. V. Dhople, B. B. Johnson, and G. B. Giannakis, "Optimal dispatch of residential photovoltaic inverters under forecasting uncertainties," *IEEE J. Photovolt.*, vol. 5, no. 1, pp. 350–359, Jan. 2015.
- [34] M. Bazrafshan and N. Gatsis, "Decentralized stochastic programming for real and reactive power management in distribution systems," in *Proc. IEEE Int. Conf. Smart Grid Communications*, Venice, Italy, Nov. 2014, pp. 218–223.
- [35] Z. Wang, B. Chen, J. Wang, M. M. Begovic, and C. Chen, "Coordinated energy management of networked microgrids in distribution systems," *IEEE Trans. Smart Grid*, vol. 6, no. 1, pp. 45–53, Jan. 2015.
- [36] T. Niknam, M. Zare, and J. Aghaei, "Scenario-based multiobjective volt/var control in distribution networks including renewable energy sources," *IEEE Trans. Power Del.*, vol. 27, no. 4, pp. 2004–2019, Oct. 2012.
- [37] S. Boyd, N. Parikh, E. Chu, B. Peleato, and J. Eckstein, "Distributed optimization and statistical learning via the alternating direction method of multipliers," *Foundations and Trends in Machine Learning*, vol. 3, no. 1, pp. 1–122, 2011.
- [38] N. Li, L. Chen, and S. H. Low, "Exact convex relaxation of opf for radial networks using branch flow model," in *Proc. IEEE Int. Conf. Smart Grid Communications*, Tainan, Nov. 2012, pp. 7–12.
- [39] A. Gomez-Exposito, A. J. Conejo, and C. Canizares, *Electric Energy Systems: Analysis and Operation*. CRC Press, 2008.